ACS Energy LETTERS

http://pubs.acs.org/journal/aelccp

LETTER

Self-Assembled Monolayer Enables Hole Transport Layer-Free Organic Solar Cells with 18% Efficiency and Improved Operational Stability

Yuanbao Lin, Yuliar Firdaus,* Furkan H. Isikgor, Mohamad Insan Nugraha, Emre Yengel, George T. Harrison, Rawad Hallani, Abdulrahman El-Labban, Hendrik Faber, Chun Ma, Xiaopeng Zheng, Anand Subbiah, Calvyn T. Howells, Osman M. Bakr, Iain McCulloch, Stefaan De Wolf, Leonidas Tsetseris, and Thomas D. Anthopoulos*

Cite This: *ACS Energy Lett.* 2020, 5, 2935−2944

Read Online

ACCESS | Metrics & More | Article Recommendations | Supporting Information

ABSTRACT: We report on bulk-heterojunction (BHJ) organic photovoltaics (OPVs) based on the self-assembled monolayer (SAM) 2PACz as a hole-selective interlayer functionalized directly onto the indium tin oxide (ITO) anode. The 2PACz is found to change the work function of ITO while simultaneously affecting the morphology of the BHJ deposited atop. Cells with PM6:N3 BHJ and ITO-2PACz anode exhibit a power conversion efficiency (PCE) of 16.6%, which is greater than that measured for bare ITO (6.45%) and ITO/PEDOT:PSS (15.94%) based devices. The enhanced performance is attributed to lower contact-resistance, reduced bimolecular recombination losses, and improved charge transport within the BHJ. Importantly, the ITO-2PACz-based OPVs show dramatically improved operational stability when compared with PEDOT:PSS-based cells. When the ITO-2PACz anode is combined with the ternary PM6:BTP-eC9:$PC_{71}BM$ BHJ, the resulting cells exhibit a maximum PCE of 18.03%, highlighting the potential of engineered SAMs for use in hole-selective contacts in high-performance OPVs.

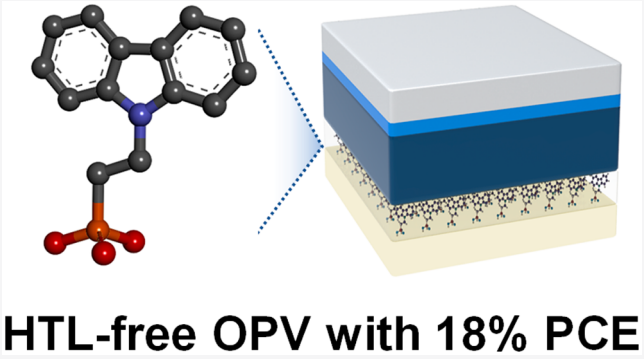

Focused research efforts in recent years have propelled the power conversion efficiencies (PCEs) of organic photovoltaics (OPVs) to over 18%.[1−5] Despite the exceptional progress, the achieved performance still lags behind the recently predicted PCE values of over 20%.[6,7] To achieve this level of performance further advances in donor and acceptor materials are needed. Equally important is the development of improved interfacial materials, not only for reaching the predicted PCE but also for enhancing the operational stability of OPVs.[8] To this end, many studies have focused on novel interfacial materials, particularly electron transport layers (ETLs) such as ZnO,[9] poly[9,9-bis(3′-(N,N-dimethyl)-N-ethylammoinium-propyl-2,7-fluorene)-alt-2,7-(9,9-dioctylfluorene)]dibromide (PFN-Br),[10] perylene diimide amino N-oxide (PDINO),[11] 3-[6-(diphenylphosphinyl)-2-naphthalenyl]-1,10-phenanthroline (Phen-NaDPO),[12] and Phen-NaDPO:$Sn(SCN)_2$.[13] In contrast, progress in hole transport layers (HTLs) currently lags behind that of ETL materials. PEDOT:PSS and its derivatives are still widely used as HTLs for standard structure OPVs,[14,15] offering multiple attractive features in terms of processability, good layer coverage, high work function (WF),[16] and tunable wettability that makes them compatible with a diverse range of bulk-heterojunction (BHJ) systems.[17] Despite the promising characteristics of PEDOT:PSS, its high acidity and hygroscopicity are known to compromise the long-term operational stability of the devices.[18,19]

Received: July 2, 2020
Accepted: August 18, 2020
Published: August 18, 2020

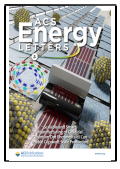

https://dx.doi.org/10.1021/acsenergylett.0c01421
ACS Energy Lett. 2020, 5, 2935−2944

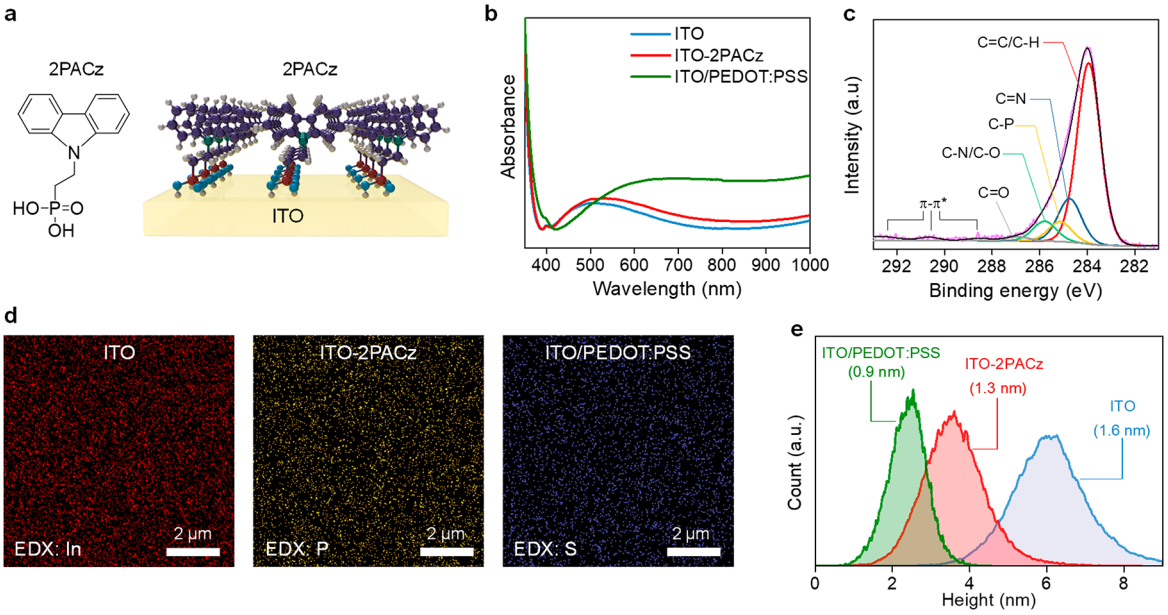

Figure 1. (a) Chemical structure of 2PACz and schematic illustration of the ITO-2PACz electrode. (b) UV−vis absorbance spectra of ITO, ITO-2PACz, and ITO/PEDOT:PSS films. (c) X-ray photoelectron spectroscopy (XPS) of the C 1s region of ITO-2PACz. (d) Elemental mapping of In (red) for ITO, P (yellow) for 2PACz, and S (blue) for PEDOT:PSS obtained using EDX (scale bar: 2 μm). (e) Surface height histograms of ITO, ITO-2PACz, and ITO/PEDOT:PSS films obtained by AFM.

HTL-free structures are currently widely used to enhance both the efficiency and stability of metal halide perovskite solar cells (PSCs), with some additional advantages including low cost, simpler fabrication, decreased parasitic absorption, and high reproducibility of PSCs.[20] Recently, self-assembled monolayers (SAMs) of organic molecules such as [2-(9*H*-Carbazol-9-yl)ethyl]phosphonic acid (2PACz) have been studied and successfully used as hole-selective contacts for HTL-free p-i-n PSCs.[20] The 2PACz SAM offers a well-suited energetic alignment and a significantly reduced nonradiative recombination at the contact/perovskite interface, leading to HTL-free PSCs with a PCE of 20.9%. These devices outperform those based on the benchmark HTL poly[bis(4-phenyl)(2,4,6-trimethylphenyl)amine] (PTAA).

Despite the demonstrated potential in PSCs, the SAM-based HTL-free approach has yet to be fully exploited in state-of-the-art OPVs.[21] To date, most studies on the use of SAMs in OPVs rely on their application as interfacial modifiers for electron-collecting cathode electrodes (see the summary of relevant literature in Table S1).[22−33] A notable example is the C_{60}-SAM-modified ZnO nanoparticles (NPs) interlayer used in nonfullerene OPVs for which simultaneous improvement of the device's PCE and photostability were achieved; the T_{80} lifetime (the time required to reach 80% of initial performance) of optimized devices was estimated to exceed 20 years.[29] In contrast, only a handful of studies have explored SAM modification of anode electrodes as a means to improve the performance of OPVs (Table S1). The lack of interest is most likely the result of low PCEs (<4%) for SAM-based OPVs as compared to state-of-the-art PEDOT:PSS-based cells.[25,26]

Here we show that 2PACz-modified ITO (ITO-2PACz) can be used as an efficient hole-collecting anode in standard architecture OPVs based on poly[(2,6-(4,8-bis(5-(2-ethylhexyl-3-fluoro)thiophen-2-yl)-benzo[1,2-b:4,5-b']-dithiophene))-*alt*-(5,5-(1′,3′-di-2-thienyl-5′,7′-bis(2-ethylhexyl)benzo[1′,2′-c:4′,5′-c']dithiophene-4,8-dione)] (PM6) and N3, as the donor polymer and nonfullerene molecular acceptor, respectively. The ensuing devices show an impressive PCE of 16.6%, which is greater than that of control cells based on bare ITO (6.45%) and optimized ITO/PEDOT:PSS-based (15.94%) anodes. We show that the presence of 2PACz increases the WF of ITO aiding hole extraction. We also find that the cells based on 2PACz-modified ITO exhibit a longer carrier lifetime, larger carrier densities, and lower bimolecular recombination compared to bare ITO and ITO/PEDOT:PSS-based OPVs. Furthermore, optical simulation of the ITO-2PACz-based cells suggests that the higher current density is due to enhanced optical field intensity within the BHJ of the device. Importantly, SAM-based OPVs also show a major improvement in their operational stability as compared to control ITO/PEDOT:PSS-based cells. To this end, our analysis shows that in comparison to ITO/PEDOT:PSS-based cells, aged ITO-2PACz-based devices retain their charge carrier mobilities and charge trapping/detrapping characteristics, ultimately leading to the limited performance degradation observed. Moreover, when the ITO-2PACz electrode is combined with the ternary PM6:BTP-eC9:PC_{71}BM BHJ, the resulting cells exhibit a remarkable maximum PCE of 18.03%, which is significantly greater than that of control cells based on PEDOT:PSS (17.52%).

The chemical structure of 2PACz and a schematic illustration of the SAM on ITO (ITO-SAM) are shown in Figure 1a. The SAM molecules attach to the metal oxide surfaces via coordination of a phosphoryl oxygen to a metallic Lewis acid.[34] In this study, the 2PACz solution (1 mg/mL in ethanol) was spin-coated directly on oxygen plasma-treated ITO resulting in strong chemisorption on its surface (Figure 1a).[35] From the UV−vis absorbance spectra in Figure 1b it is evident that the ITO-2PACz exhibits lower absorbance than the conventional ITO/PEDOT:PSS anode electrode in the ranges from 350 to 415 nm and 500 to 1000 nm, which could be beneficial for application in OPVs and will be discussed later.

https://dx.doi.org/10.1021/acsenergylett.0c01421
ACS Energy Lett. 2020, 5, 2935−2944

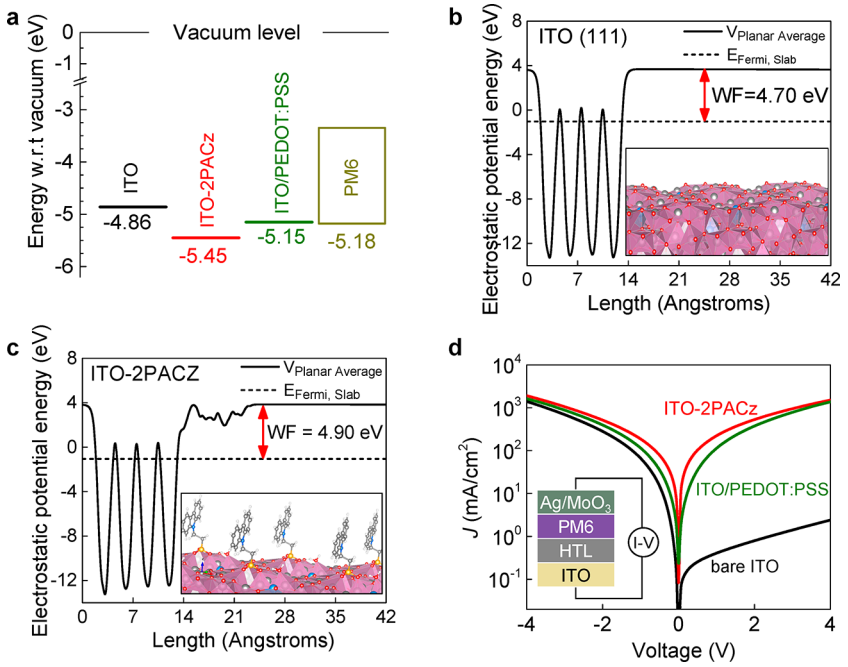

Figure 2. (a) Work function of ITO, ITO-2PACz, ITO/PEDOT:PSS, and HOMO level of PM6 measured via the photoelectron spectroscopy in air (PESA) technique. Calculated electrostatic potentials for (b) the (111) surface of ITO and (c) the surface of ITO with a 2PACz SAM (results obtained with DFT slab calculations on supercells with stoichiometry $In_{60}Sn_4O_{96}$). The inset shows side views of the structures (In, gray; Sn, blue; O, red; C, light gray; N, blue; P, orange; H, white spheres). (d) Dark current through a hole-only device based on ITO, 2PACz, and PEDOT:PSS. The inset shows the schematic of the hole-only cell's architecture.

With the aid of density functional theory (DFT) calculations, we confirmed that there exist several chemisorption configurations, with bidentate or tridentate types of binding between the 2PACz molecules and the ITO surface, as shown in Figure S1. Based on the calculated energies, the most stable chemisorbed structure is shown in Figure S1a and entails a tridentate pattern with covalent bonds between all three acidic O atoms of a 2PACz molecule and an underlying substrate atom. In an effort to detect direct evidence of the presence of atomic species related to 2PACz on the surface of ITO, we utilized X-ray photoelectron spectroscopy (XPS). Figure S2a shows the XPS data in the whole scan region (0–700 eV). The existence of signals related to N and P can directly be attributed to the presence of 2PACz molecules, while the strong presence of In originates from the ITO electrode beneath because of the monolayer nature of the 2PACz SAM.

Figure 1c shows the high-resolution C 1s binding energy region for the ITO-2PACz electrode, showing a characteristic signal of the 2PACz and its carbazole component.[36,37] The measured spectra can be satisfactory fit with five main peaks (287–282 eV) with a mixed Lorentzian/Gaussian line shape and a Shirley background. The additional peaks between 288 and 293 eV originate from $\pi-\pi^*$ shakeup satellite loss.[37] The peak at 284.7 eV with a relative peak area of 0.155 is assigned to the C=N bond in the carbazole unit of the 2PACz, while the peak at 285.8 eV with a relative area of 0.074 is attributed to the C–N bond in the aliphatic linking chain.[37] The peak at 285.2 eV with a relative peak area of 0.071, on the other hand, is assigned to the C–P bond in agreement with the literature.[38,39] The scaling of relative peak areas is in line with the number of relevant atoms present in 2PACz (Figure 1a). A small contribution from adventitious C–O (~286 eV) cannot be excluded and most likely overlaps with the signal originating from C–N.

The coverage of 2PACz on ITO can be estimated using different methods, including cyclic voltammetry[40] and XPS.[41,42] In the present study we employed the XPS technique because of its availability in our laboratory. As explained in detail in the Supporting Information, the ratio of P(2p)/In($3d_{5/2}$) signals is predicted for a close-packed 2PACz ($\theta = 1$) overlayer on an ITO surface after accounting for electron attenuation, atomic density, and core level sensitivity (Figure S2 and Table S2).[43] Overall, an average coverage of 0.92 $\theta \pm$ 0.1 θ is determined, equating to ~4.05×10^{14} molecules/cm^2. The latter value is in line with that measured by Paniagua et al. for a saturated phosphonic acid/ITO surface.[41] This analysis supports the facile formation of a highly dense coverage of 2PACz and a suitable hole contact interface. Further evidence of the presence of 2PACz on the ITO surface was obtained by energy-dispersive X-ray spectroscopy (EDX) measurements (Figure 1d). The measured distribution of P (EDX: P) on ITO suggests a high coverage by the 2PACz SAM, as would be expected for a dense monolayer, and is qualitatively similar to that observed for the S distribution in the ITO/PEDOT:PSS (EDX: S) electrode. All aforementioned results suggest that 2PACz functionalized on the surface of ITO, forming a dense monolayer.

Atomic force microscopy (AFM) was also used to study the surface topography of ITO, ITO-2PACz, and ITO/PEDOT:PSS anode electrodes. Figure S3 shows the AFM images, while Figure 1e displays the corresponding surface height histograms extracted from those images. The ITO-2PACz electrode exhibits a smoother surface than bare ITO, which is manifested in the slightly lower root-mean-square (RMS) surface roughness value of 1.3 nm (ITO = 1.6 nm) and shifts the entire distribution toward smaller height values. The ITO/

https://dx.doi.org/10.1021/acsenergylett.0c01421
ACS Energy Lett. 2020, 5, 2935–2944

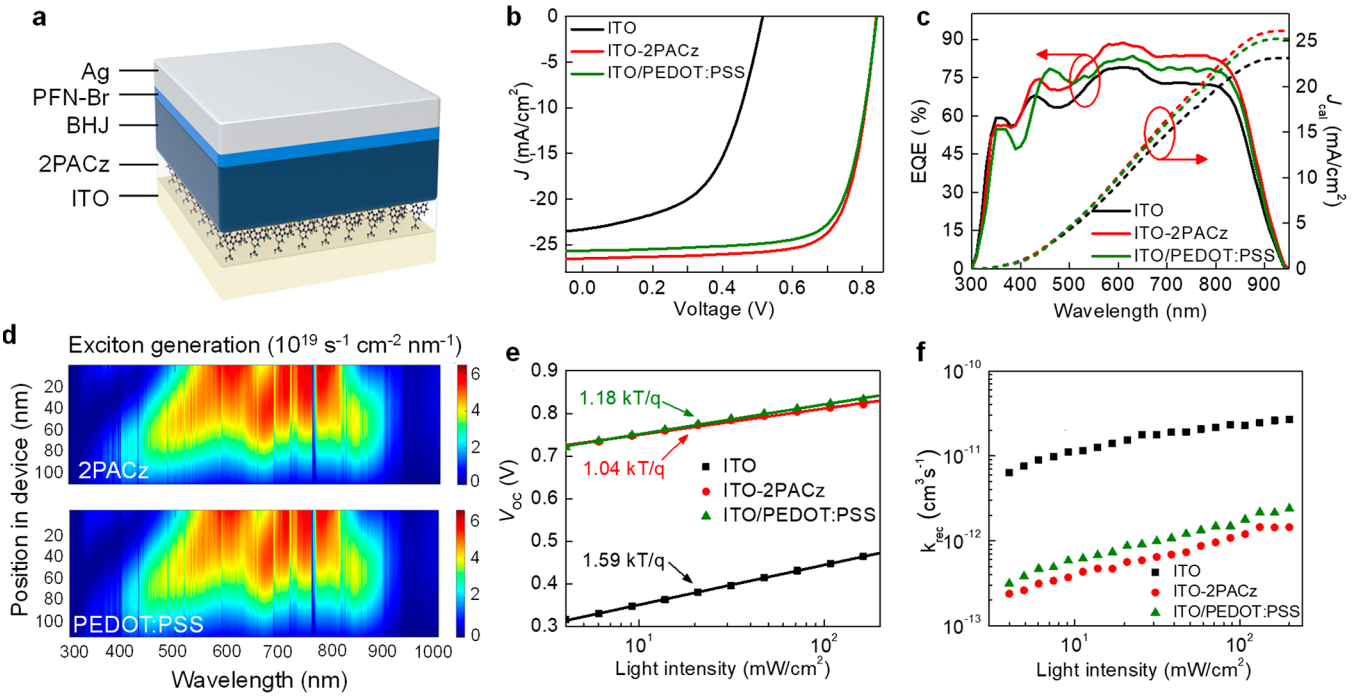

Figure 3. (a) Schematic of the standard cell architectures employed. (b) $J-V$ curves of PM6:N3 solar cells based on ITO, ITO-2PACz, and ITO/PEDOT:PSS. (c) External quantum efficiency (EQE) curves of the same OPV. (d) Optical simulations for the exciton generation rate profiles in the studied SAM and PEDOT:PSS-based OPV devices. Light intensity dependence of (e) V_{OC} and (f) bimolecular recombination rate constant (k_{rec}) for the same cells.

PEDOT:PSS electrode appears significantly smoother with a surface RMS of 0.89 nm due to the narrower height distribution.

Next, we used photoelectron spectroscopy in air (PESA) to determine the WF of ITO electrode before and after 2PACz functionalization (Figure S4 and Table S3). As shown in Figure 2a, the WF of ITO-2PACz (−5.45 eV) is significantly deeper than the value measured for the bare ITO (−4.86 eV) and ITO/PEDOT:PSS (−5.15 eV) electrodes. Kelvin probe measurements confirm the WF trend revealed by the PESA measurements (see comparison in Table S3). We have also evaluated the WF for all pertinent electrode structures using DFT calculations (Figure 2b,c). For the bare (111) ITO surface, we derive a WF of −4.70 eV, which is in good agreement with the experimentally determined value, i.e., −4.86 eV. For the same ITO surface functionalized with 2PACz in the configuration shown in Figure S1a, and considering a surface coverage of 5.04×10^{13} molecules/cm^2, we calculate a WF of −4.90 eV. The latter value agrees with the trend of an increased WF upon functionalization, albeit to a lesser extent compared to the experimentally measured change described above. We note, however, that previous studies of Hotchkiss et al. found a monotonic increase of the absolute values of the WF as a function of the coverage of ITO surfaces functionalized with phosphonic acids.[44] Hence, our calculated WF (−4.90 eV) for the relative low 2PACz coverage (5.04×10^{13} molecules/cm^2) is consistent with the measured WF (−5.45 eV) at higher coverages (4.05×10^{14} molecules/cm^2).

To investigate the impact of 2PACz functionalization on the characteristics of hole-injection from an ITO electrode into an organic semiconductor, we fabricated hole-only devices. Figure 2d shows the dark current−voltage curves for a hole-only device based on the donor polymer PM6, while the inset shows the schematic of the device architecture employed. Here, PM6 is sandwiched between either ITO, ITO/PEDOT:PSS or ITO-2PACz, and an Ohmic hole-injecting Ag/MoO_3 contact. Because the PM6 is characterized by a moderately deep highest occupied molecular orbital (HOMO) energy level of 5.18 eV (Figure 2a), hole injection from ITO (WF = −4.86 eV) is expected to be suppressed because of the presence of a substantial potential barrier of ∼0.32 eV. As evident from Figure 2d, the current injected from bare ITO (forward bias) is indeed significantly lower than that injected from the Ohmic hole-injecting Ag/MoO_3 contact under reverse bias. The hole injection improves drastically upon inserting either a 40 nm thick layer PEDOT:PSS between ITO and PM6 or by functionalizing the 2PACz SAM onto ITO. In both cases, a remarkable transition from highly asymmetric (bare ITO) to nearly symmetric forward and reverse $J-V$ curves occurs, highlighting the hole-transport enabling role of PEDOT:PSS and 2PACz. Importantly, devices utilizing ITO-2PACz as the hole-injecting electrode exhibit slightly higher current than those based on PEDOT:PSS, especially at lower biasing levels, possibly indicating an improved Ohmic contact as compared to PEDOT:PSS. In addition, the maximum hole mobility (μ_h), calculated via the space-charge limited current (SCLC) method, for the 2PACz-based device is slightly higher (1.1×10^{-3} cm^2 V^{-1} s^{-1}) than PEDOT:PSS-based devices (9.1×10^{-4} cm^{2}V^{-1}s^{-1}), further supporting the existence of an improved hole-injecting contact in the case of ITO-2PACz.

The surface energy of ITO/HTL is another significant parameter that affects the morphology of the BHJ layer in OPVs. We performed contact-angle measurements for ITO and ITO-2PACz (Figure S5), from which the surface energies were inferred using the Owens equation[45]

$$\gamma_l(1 + \cos\theta) = 2(\gamma_s^D \gamma_l^D)^{1/2} + 2(\gamma_s^P \gamma_l^P)^{1/2} \quad (1)$$

https://dx.doi.org/10.1021/acsenergylett.0c01421
ACS Energy Lett. 2020, 5, 2935−2944

Table 1. Summary of Key Operating Parameters of OPVs Based on PM6:N3 BHJs with Different Anode Electrode Systems Measured under Illumination of AM 1.5G (100 mW/cm^2)

Anode electrode	V_{OC} [V]	J_{SC} [mA/cm^2]	J_{cal} [mA/cm^2]	FF [%]	PCE [%]	R_S [Ω cm^2]
ITO (bare)	0.515	23.32	23.15	53.7	6.45 (5.93 ± 0.38)[a]	5.30
ITO-2PACz	0.840	26.53	26.14	74.5	16.60 (16.30 ± 0.22)	2.47
ITO/PEDOT:PSS	0.842	25.64	25.28	73.9	15.94 (15.72 ± 0.14)	2.94

[a]PCE_{avg} values in parentheses represent averages from 15 devices.

here γ_l is the surface energy of liquid, which is composed of dispersion component γ and polarity component γ. Similarly, γ_s is the surface energy of solid, which is composed of dispersion component γ and polarity component γ. The results are summarized in Table S4 and show that the ITO-2PACz has a higher surface energy (68.7 mN/m) than both the bare ITO (57.9 mN/m) and ITO/PEDOT:PSS (59.8 mN/m) electrodes, suggesting the possibility of a stronger interaction between the BHJ solution and the ITO-2PACz surface during spin-coating. To probe this further we used AFM to measure the surface morphology of the PM6:N3 layer. The chemical structure and energy levels of the materials are shown in Figure S6, while Figure S7 presents the AFM images and surface height histogram for the BHJ deposited onto the various surfaces. The PM6:N3 BHJ deposited on bare ITO exhibit a relatively broad rough surface (RMS = 2.3 nm). In contrast, ITO/PEDOT:PSS and ITO-2PACz show more homogeneous morphologies and lower surface roughness of 1.5 and 1.2 nm, respectively. This trend is better illustrated in the surface height histograms of Figure S7d, where the height distribution for the BHJ on ITO-2PACz undergoes a clear shift toward lower heights, indicating surface smoothening. Moreover, both the topography and phase images reveal the existence of a nanofiber structure in the PM6:N3 BHJ layer, deposited onto ITO-2PACz electrodes. The latter is most likely the result of a particular interaction between the semiconductor solution and the ITO-2PACz electrode surface during spin coating. The different BHJ morphology is expected to lead to different optoelectronic properties, which are discussed later.

To explore the potential of 2PACz as a possible replacement for PEDOT:PSS in OPVs, we fabricated HTL-free cells based on the standard architecture shown in Figure 3a using PM6:N3 as the BHJ. The experimental conditions used to functionalize the 2PACz onto ITO (e.g., annealing temperatures and plasma cleaning time) were carefully optimized, and the results are summarized in Figures S8−S10 and Tables S5−S7. Representative $J-V$ curves obtained from the resulting OPV cells are shown in Figure 3b, while a summary of the key device parameters is provided in Table 1. Cells with bare ITO exhibit a maximum PCE of 6.45% with a short-circuit current (J_{SC}) of 23.32 mA/cm^2, an open circuit voltage (V_{OC}) of 0.515 V, a fill factor (FF) of 53.7%, and series resistance (R_S) of 5.30 Ω cm^2. OPVs based on ITO/PEDOT:PSS show improved performance with a maximum PCE of 15.94%, which is comparable to the published result for PM6:N3 BHJ OPVs (15.98%) based on the standard device architecture.[46] Remarkably, when 2PACz SAM was applied atop of ITO (ITO-2PACz), the PCE increases to 16.6%, accompanied by an increased J_{SC} (26.53 mA/cm^2), an improved FF (74.5%), and a reduced R_S (2.47 Ω cm^2).

Figure 3c displays the external quantum efficiency (EQE) spectra of the PM6:N3-based OPV cells. For all devices, the integrated current density (J_{cal}) deduced from the EQE spectra matches well the values obtained from the $J-V$ measurements within ±1.5% (Table 1). The ultrathin nature of the 2PACz SAM functionalized on ITO enables cells with a higher photoresponse in the ranges of 345−440 nm and 510−860 nm, as compared to ITO/PEDOT:PSS-based cells, ultimately resulting in higher J_{cal} (Figure 3c). This significant enhancement likely arises from the lower absorbance of the ITO-2PACz compared to ITO/PEDOT:PSS anodes (Figure 1b). Figure S11 overlays internal quantum efficiency (IQE) spectra, removing the dependence on optical absorption. The average IQEs of an OPV with ITO-2PACz equal to 90.5% for the spectral range 450−850 nm, reaching up to 98.8% at 570 nm. In comparison, the average IQEs for the OPV with PEDOT:PSS is 85.9% in the same range. The higher average IQEs from SAM-based devices suggests that most of the absorbed photons are converted to free carriers with higher efficiency and then collected at the corresponding electrodes.

To better understand the influence of 2PACz and PEDOT:PSS on the optical properties of the cells, we simulated the optical field intensity across the device using the transfer-matrix formalism.[47] The optical constants (refractive index n and extinction coefficient k) for all layers in the device were measured independently using spectroscopic ellipsometry (Figure S12a,b). As shown in Figures 3d and S12c−e, the cell based on ITO-2PACz exhibits a higher optical electric field intensity and exciton generation rate within the BHJ and a lower parasitic absorption than the ITO/PEDOT:PSS device. These calculations corroborate the experimental results and further highlight the potential of ITO-2PACz for application in high-performance OPVs. The calculated maximum J_{SC} (IQE = 100%) of SAM-based devices (Figure S12f) exceeds PEDOT:PSS-based cells when BHJ thickness is grater than 80 nm, in agreement with $J-V$ results in Figure 3b.

Next, the impact of 2PACz on charge-carrier recombination in the devices was studied via light-intensity-dependent $J-V$ measurements, transient photovoltage (TPV), and charge-extraction (CE) measurements (Figure S13a−c). Figure 3e shows the variation of V_{OC} versus light intensity plotted on a semilogarithmic scale with the data fitted to $V_{OC} \propto SkT/q \ln(I)$, where S, k, T, q, and I are the slope, Boltzmann constant, temperature, elementary charge, light intensity, respectively. If trap-assisted recombination is involved, a stronger dependence of V_{OC} on the light intensity with a slope greater than kT/q will be observed.[48] The dependence of V_{OC} on the light intensity for the ITO-2PACz cells exhibits a slope of 1.04 kT/q, which is significantly smaller than the 1.59 kT/q measured for bare ITO-based devices, and still lower than 1.18 kT/q measured for the optimized ITO/PEDOT:PSS-based cell. These results highlight the ability of the ITO-2PACz anode to reduce the trap-assisted recombination, which is partly reflected in the improved PCE.

Further insights into the charge carrier dynamics were obtained by measuring the charge carrier lifetime (τ) and carrier density using TPV and CE measurements, respectively,

https://dx.doi.org/10.1021/acsenergylett.0c01421
ACS Energy Lett. 2020, 5, 2935−2944

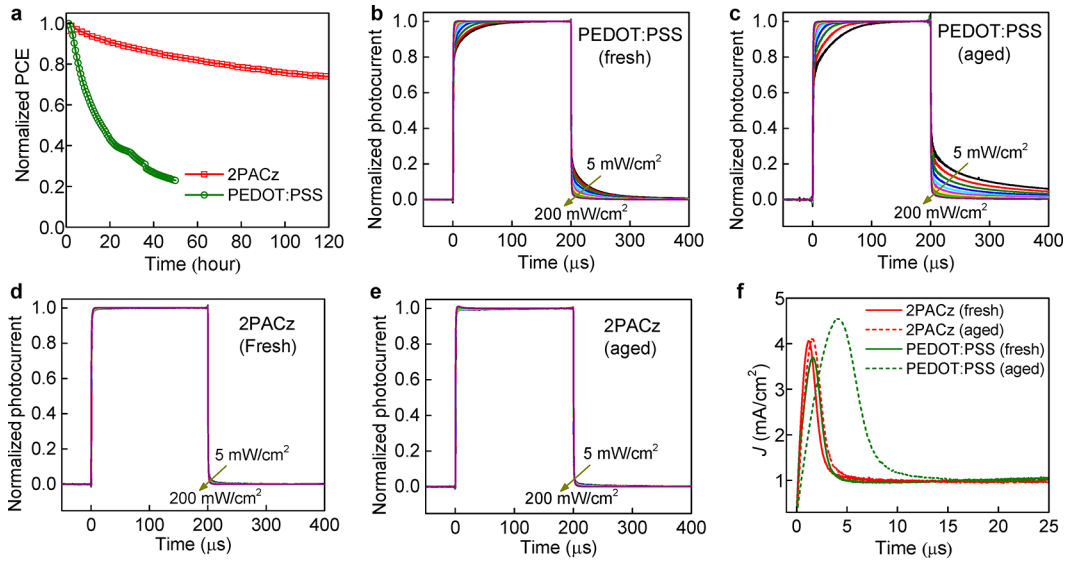

Figure 4. (a) Evolution of normalized PCEs of PM6:N3-based BHJ OPVs based on ITO-2PACz and ITO/PEDOT:PSS anodes under maximum power point tracking (MPPT) testing. Transient short-circuit photocurrent of fresh and aged OPVs based on ITO/PEDOT:PSS (b and c) and ITO-2PACz-based cell (d and e). (f) Photo-CELIV traces measured for fresh and aged ITO-2PACz and ITO/PEDOT:PSS-based cells.

under varying light intensity conditions (Figure S13d,e).[49] The carrier lifetime in ITO-2PACz-based devices is found to be consistently longer across the entire light intensity range investigated. Representative values include those measured at 200 mW/cm^2 yielding 2.7 μs for ITO-2PACz, 1.8 μs for ITO/PEDOT:PSS, and 0.4 μs for bare ITO (Figure S13d). The consistently larger τ for ITO-2PACz-based cells is indicative of a lower carrier recombination. Interestingly, higher carrier densities are also measured for OPVs with ITO-2PACz as compared to ITO/PEDOT:PSS and bare ITO-based cells, in line with the higher J_{SC} (Table 1). We also inferred the bimolecular recombination rate constants (k_{rec}) from the carrier lifetime and densities according to $k_{rec} = 1/[(\lambda+1)n\tau]$, where λ is the recombination order.[50] As shown in Figure 3f, k_{rec} for the ITO-2PACz device is lower than that measured for the bare ITO and ITO/PEDOT−PSS-based cells at all light densities investigated.

Electrochemical impedance spectroscopy (EIS) measurements were performed to examine the interface resistance in the various OPVs in the dark while applying a bias voltage equal to V_{OC}.[51] Nyquist plots shown in Figure S14 were fitted by using the equivalent circuit model following a previous report,[52] and the relevant data are summarized in Table S8. The interface resistances (R_2) of the devices with bare ITO, ITO-2PACz, and ITO/PEDOT:PSS are estimated to be 540.4, 37.8, and 43.5 Ω, respectively. The results show the advantage of ITO-2PACz to enable a lower interface resistance thanks to its deeper WF, ultimately leading to cells with higher FF and overall PCE.[16,53] Furthermore, the average carrier transition time (τ_{avg}) of the equivalent circuit was calculated using[52]

$$\tau_{avg} = R_1 \times C_1 \quad (2)$$

where R_1 and C_1 are the resistance and capacitance of the active layer, respectively. The calculated τ_{avg} values for OPVs based on bare ITO, ITO-2PACz, and ITO/PEDOT:PSS anodes are 0.4, 3.1, and 2.1 μs, respectively, and are consistent with the τ values calculated from TPV measurements.

We have also investigated the operational stability of optimized PM6:N3 OPVs based on different anode electrodes given its paramount importance for any practical application of the technology.[54,55] We performed maximum power point tracking (MPPT) measurements while storing the devices under vacuum. A tracking step of 60 s was used while the device was subjected to continuous illumination supplied by a white color light-emitting diode (LED) with a light intensity of 200 mW/cm^2. The normalized PCE plotted as a function of light-soaking time is presented in Figure 4a. After 120 h of continuous light soaking, the ITO-2PACz-based cell retains 74% of its initial PCE, while the performance of the PEDOT:PSS-based cell deteriorates rapidly to ∼20% of its initial PCE after 50 h. Although preliminary, the results indicate that ITO-2PACz could potentially help to enhance the lifetime of state-of-the-art OPVs.

To gain better insight into the device degradation mechanism, both fresh and aged devices were analyzed using transient photocurrent (TPC) measurements, a highly versatile technique often used to study space-charge effects, carrier trapping, and detrapping in OPVs. Here, cells are excited with a square-shaped light pulse of varying intensity (5−200 mW/cm^2) and long enough (200 μs) for the photocurrent to reach a steady state. The recorded TPC traces can then be analyzed according to three key features: (i) the initial rapid rise time, (ii) the time needed for the photocurrent to reach a quasi-steady-state, and (iii) the fall time of the photocurrent. Freshly prepared ITO/PEDOT:PSS devices exhibit fast rise and fall time response to the light pulse (Figure 4b). Following aging, however, the same device exhibits significantly slower rise and fall times, an effect particularly pronounced at illumination intensities of <30 mW/cm^2 (Figure 4c). The latter suggests the presence of a higher number of deep electron trap states that have been formed during device aging.[56,57] In contrast, no obvious change in the characteristic features of the TPC traces measured for fresh (Figure 4d) and aged (Figure 4e) ITO-2PACz-based cells was found. The only noticeable difference is the slight current overshoots seen at high light intensity

https://dx.doi.org/10.1021/acsenergylett.0c01421
ACS Energy Lett. 2020, 5, 2935−2944

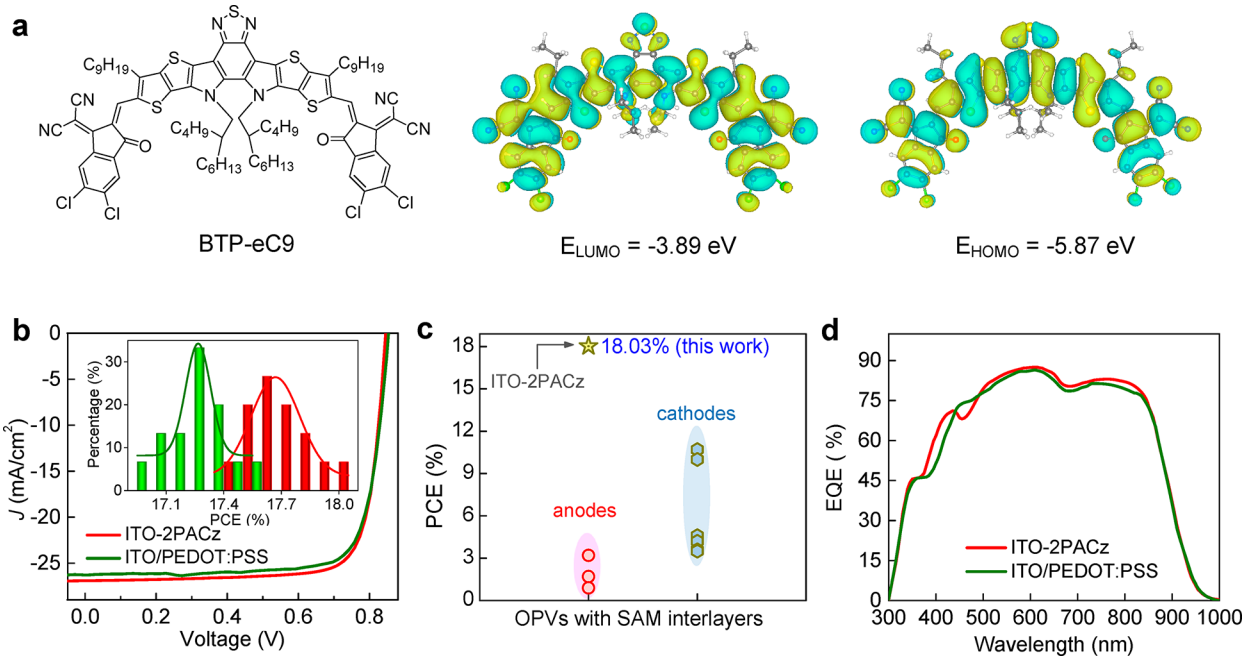

Figure 5. (a) Molecular structure of BTP-eC9, and its HOMO and LUMO calculated via DFT. (b) $J-V$ curves of PM6:BTP-eC9:$PC_{71}BM$ solar cells based on ITO-2PACz and ITO/PEDOT:PSS. The inset in panel b shows the histogram and Gaussian fit (solid lines) of PCEs measured for OPVs with ITO-2PACz (red) and ITO/PEDOT:PSS (green). (c) A summary of reported PCE values for SAM-modified OPVs.[22−33] (d) EQE curves of the same OPV devices.

Table 2. Summary of Key Operating Parameters of OPVs Based on PM6:BTP-eC9:$PC_{71}BM$ BHJs with Different Anode Electrode Systems Measured under Illumination of AM 1.5G (100 mW/cm²)

Anode electrode	V_{OC} [V]	J_{SC} [mA/cm²]	J_{cal} [mA/cm²]	FF [%]	PCE [%]	R_S [Ω cm²]
ITO-2PACz	0.845	26.94	26.65	79.2	18.03 (17.70 ± 0.16)[a]	1.52
ITO/PEDOT:PSS	0.854	26.28	26.02	78.2	17.52 (17.52 ± 0.15)	2.23

[a]PCE_{avg} values in brackets represent averages from 15 devices.

measurements for the aged ITO-2PACz-based OPV, a feature previously attributed to a change in the BHJ morphology.[58] Nevertheless, the changes in the TPC traces for ITO-2PACz-based cells is negligible when compared to ITO/PEDOT:PSS devices, which explains the enhanced operational stability of ITO-2PACz-based OPV cells.

We also studied the impact of aging on the charge carrier mobility (μ) using the photogenerated charge extraction by a linearly increasing voltage (photo-CELIV) technique.[59] From the measured photocurrent transients (Figure 4f) the carrier mobility can be calculated using

$$\mu = 2d^2/(3At_{max}^2(1 + 0.36\Delta j/j_0)) \quad (3)$$

where d is BHJ thickness, A the voltage rise speed of the applied voltage pulse, and t_{max} the time to reach the extraction current maximum; Δj and j_0 are the displacement and initial currents, respectively. The photo-CELIV extracted mobilities for the fresh ITO-2PACz and PEDOT:PSS-based cells are 2.55×10^{-4} and 1.87×10^{-4} cm² V^{-1} s^{-1}, respectively. The higher device mobility in ITO-2PACz-based device most likely originates from the difference in the BHJ morphology and particularly to the presence of fiber-like features seen in the AFM images of Figure S7b. Following aging, the μ value in ITO-2PACz-based cells decreases slightly to 1.98×10^{-4} cm² V^{-1} s^{-1}, while for aged ITO/PEDOT:PSS devices the drop is significantly larger (8.78×10^{-5} cm² V^{-1} s^{-1}). Once again, the results highlight the superiority of ITO-2PACz-based cells over ITO/PEDOT:PSS-based devices.

To elucidate the origin of the improved stability of SAM-based cells, EIS measurements were used to study the electrical properties of the aged ITO-2PACz/BHJ and PEDOT:PSS/BHJ interfaces (Figure S14 and Table S8).[52] Both ITO-2PACz and ITO/PEDOT:PSS-based cells exhibit similar trends of increased BHJ resistances and decreased BHJ capacitances, suggesting that the degradation of the active layer is not the primary reason for the differences seen in the operational stability between the two cells (Figure 4a). However, the significantly increased interface (43.5 Ω vs 306.4 Ω) and electrode (17.4 Ω vs 57.8 Ω) resistance values observed for the PEDOT:PSS-based OPVs following MPPT measurements, indicate that the interface has deteriorated. In contrast, for ITO-2PACz-based OPVs subjected to MPPT testing, the interface and electrode resistance changes are significantly smaller (37.8 Ω vs 42.1 Ω and 15.6 Ω vs 31.8 Ω, respectively), suggesting the existence of a more stable ITO-2PACz/BHJ interface.

Recently, the nonfullerene acceptor BTP-eC9 has helped to increase the PCE of single-junction OPV cells close to 18%.[1] The chemical structure, HOMO, and LUMO energies *via* DFT of BTP-eC9 is presented in Figure 5a. To study the compatibility of the proposed ITO-2PACz anode with PM6:BTP-eC9:$PC_{71}BM$, we prepared a series of OPV cells based on ITO/PEDOT:PSS and ITO-2PACz anodes. Figure

https://dx.doi.org/10.1021/acsenergylett.0c01421
ACS Energy Lett. 2020, 5, 2935−2944

S15 and Table S9 summarize the different weight ratio (wt %) used for optimizing the PM6:BTP-eC9:$PC_{71}BM$ system. As shown in Figure 5b and Table 2, cells with PEDOT:PSS HTL yield V_{OC} of 0.854 V, J_{SC} of 26.28 mA/cm^2, and a FF of 78.2%, resulting in a maximum PCE of 17.52%. Remarkably, OPVs based on ITO-2PACz anodes show a higher maximum PCE value of 18.03%, accompanied by a slightly lower V_{OC} (0.845 V), an increased J_{SC} (26.94 mA/cm^2), and an enhanced FF (79.2%). The PCE of 18.03% is the highest PCE reported to date for OPVs utilizing SAMs either as part of the hole- or the electron-collecting electrode (see summary in Figure 5c and Table S1).[22−33] The statistical PCE values from 15 devices (see insert in Figure 5b) demonstrate the reproducibility of these high PCE devices. Moreover, the EQE spectra (Figure 5d) exhibits a higher photoresponse in the ranges of 380−430 nm and 500−800 nm, compared to ITO/PEDOT:PSS-based cells, ultimately contributing to the higher J_{cal} (26.65 mA/cm^2 vs 26.02 mA/cm^2) in Table 2. This trend of enhanced EQE response is similar to that measured for PM6:N3 cells employing ITO-2PACz anodes (Figure 3c).

In conclusion, we have successfully integrated the 2PACz SAM as a hole-selective interlayer in HTL-free BHJ OPVs. The functionalization of 2PACz from solution directly onto ITO was found to increase its work function and decrease the contact resistance with the BHJ layer. AFM analysis showed that solution-processing of the PM6:N3 BHJ onto ITO-2PACz anode electrodes affects the BHJ layer morphology, resulting in a nanofibrous surface texture. Solar cells based on PM6:N3 BHJ and 2PACz-modified ITO yielded a maximum PCE of 16.60%, a higher value than control cells based on PEDOT:PSS (15.94%). Analysis of the carrier recombination dynamics revealed that the enhanced performance is primarily due to improved optical absorption within the BHJ and enhanced charge extraction. Importantly, the ITO-2PACz-based OPVs showed remarkably enhanced operational stability as compared to ITO/PEDOT:PSS-based cells. The ITO-2PACz-based cell retained 74% of its initial performance after 120 h MPPT, while the ITO/PEDOT:PSS devices degraded to 20% of their preaging performance level after 50 h of MPPT. The improved stability was attributed to negligible change in the interface between ITO-2PACz and the BHJ, as well as the ability of the cells to maintain the high charge-carrier mobility before and after photoaging. Finally, the broader applicability of the ITO-2PACz anode was demonstrated with its application in OPVs based on PM6:BTP-eC9:$PC_{71}BM$ as the BHJ, exhibiting a PCE of 18.03%, which is the highest reported to date for SAM-based OPVs. Our work highlights ITO-2PACz as a cost-effective hole-selective contact technology for application in stable, high-efficiency OPVs.

■ ASSOCIATED CONTENT

Supporting Information

The Supporting Information is available free of charge at https://pubs.acs.org/doi/10.1021/acsenergylett.0c01421.

Fabrication and characterization details of OPVs, methodology for DFT calculations, XPS analysis, AFM measurements, PESA measurements, contact angle and surface energy characteristics, optimization of 2PACz-based OPVs, optical simulation, and light intensity characterization of OPVs (PDF)

■ AUTHOR INFORMATION

Corresponding Authors

Yuliar Firdaus − *King Abdullah University of Science and Technology (KAUST), KAUST Solar Center (KSC), Thuwal 23955, Saudi Arabia*; Email: yuliar.firdaus@kaust.edu.sa

Thomas D. Anthopoulos − *King Abdullah University of Science and Technology (KAUST), KAUST Solar Center (KSC), Thuwal 23955, Saudi Arabia*; orcid.org/0000-0002-0978-8813; Email: thomas.anthopoulos@kaust.edu.sa

Authors

Yuanbao Lin − *King Abdullah University of Science and Technology (KAUST), KAUST Solar Center (KSC), Thuwal 23955, Saudi Arabia*

Furkan H. Isikgor − *King Abdullah University of Science and Technology (KAUST), KAUST Solar Center (KSC), Thuwal 23955, Saudi Arabia*

Mohamad Insan Nugraha − *King Abdullah University of Science and Technology (KAUST), KAUST Solar Center (KSC), Thuwal 23955, Saudi Arabia*; orcid.org/0000-0001-9352-1902

Emre Yengel − *King Abdullah University of Science and Technology (KAUST), KAUST Solar Center (KSC), Thuwal 23955, Saudi Arabia*; orcid.org/0000-0001-7208-4803

George T. Harrison − *King Abdullah University of Science and Technology (KAUST), KAUST Solar Center (KSC), Thuwal 23955, Saudi Arabia*

Rawad Hallani − *King Abdullah University of Science and Technology (KAUST), KAUST Solar Center (KSC), Thuwal 23955, Saudi Arabia*

Abdulrahman El-Labban − *King Abdullah University of Science and Technology (KAUST), KAUST Solar Center (KSC), Thuwal 23955, Saudi Arabia*

Hendrik Faber − *King Abdullah University of Science and Technology (KAUST), KAUST Solar Center (KSC), Thuwal 23955, Saudi Arabia*

Chun Ma − *King Abdullah University of Science and Technology (KAUST), KAUST Solar Center (KSC), Thuwal 23955, Saudi Arabia*

Xiaopeng Zheng − *King Abdullah University of Science and Technology (KAUST), Physical Science and Engineering Division (PSE), Thuwal 23955, Saudi Arabia*

Anand Subbiah − *King Abdullah University of Science and Technology (KAUST), KAUST Solar Center (KSC), Thuwal 23955, Saudi Arabia*; orcid.org/0000-0002-7505-3209

Calvyn T. Howells − *King Abdullah University of Science and Technology (KAUST), KAUST Solar Center (KSC), Thuwal 23955, Saudi Arabia*

Osman M. Bakr − *King Abdullah University of Science and Technology (KAUST), Physical Science and Engineering Division (PSE), Thuwal 23955, Saudi Arabia*; orcid.org/0000-0002-3428-1002

Iain McCulloch − *King Abdullah University of Science and Technology (KAUST), KAUST Solar Center (KSC), Thuwal 23955, Saudi Arabia*

Stefaan De Wolf − *King Abdullah University of Science and Technology (KAUST), KAUST Solar Center (KSC), Thuwal 23955, Saudi Arabia*; orcid.org/0000-0003-1619-9061

Leonidas Tsetseris − *Department of Physics, National Technical University of Athens, Athens GR-15780, Greece*

Complete contact information is available at: https://pubs.acs.org/10.1021/acsenergylett.0c01421

https://dx.doi.org/10.1021/acsenergylett.0c01421
ACS Energy Lett. 2020, 5, 2935−2944

Notes

The authors declare no competing financial interest.

■ ACKNOWLEDGMENTS

This publication is based upon work supported by the King Abdullah University of Science and Technology (KAUST) Office of Sponsored Research (OSR) under Award No. OSR-2018-CARF/CCF-3079. L.T. acknowledges support for the computational time granted from GRNET in the National HPC facility -ARIS - under project SPOx.

■ REFERENCES

(1) Cui, Y.; Yao, H.; Zhang, J.; Xian, K.; Zhang, T.; Hong, L.; Wang, Y.; Xu, Y.; Ma, K.; An, C.; He, C.; Wei, Z.; Gao, F.; Hou, J. Single-Junction Organic Photovoltaic Cells with Approaching 18% Efficiency. *Adv. Mater.* **2020**, *32* (19), 1908205.

(2) Liu, Q. S.; Jiang, Y. F.; Jin, K.; Qin, J. Q.; Xu, J. G.; Li, W. T.; Xiong, J.; Liu, J. F.; Xiao, Z.; Sun, K.; Yang, S. F.; Zhang, X. T.; Ding, L. M. 18% Efficiency organic solar cells. *Sci. Bull.* **2020**, *65* (4), 272−275.

(3) Liu, L.; Kan, Y. Y.; Gao, K.; Wang, J. X.; Zhao, M.; Chen, H.; Zhao, C. J.; Jiu, T.; Jen, A. K. Y.; Li, Y. L. Graphdiyne Derivative as Multifunctional Solid Additive in Binary Organic Solar Cells with 17.3% Efficiency and High Reproductivity. *Adv. Mater.* **2020**, *32* (11), 1907604.

(4) Lin, Y.; Firdaus, Y.; Nugraha, M. I.; Liu, F.; Karuthedath, S.; Emwas, A. H.; Zhang, W.; Seitkhan, A.; Neophytou, M.; Faber, H.; Yengel, E.; McCulloch, I.; Tsetseris, L.; Laquai, F.; Anthopoulos, T. D. 17.1% Efficient Single-Junction Organic Solar Cells Enabled by n-Type Doping of the Bulk-Heterojunction. *Adv. Sci.* **2020**, *7* (7), 1903419.

(5) Lin, Y.; Adilbekova, B.; Firdaus, Y.; Yengel, E.; Faber, H.; Sajjad, M.; Zheng, X.; Yarali, E.; Seitkhan, A.; Bakr, O. M.; El-Labban, A.; Schwingenschlogl, U.; Tung, V.; McCulloch, I.; Laquai, F.; Anthopoulos, T. D. 17% Efficient Organic Solar Cells Based on Liquid Exfoliated WS_2 as a Replacement for PEDOT:PSS. *Adv. Mater.* **2019**, *31* (46), 1902965.

(6) Firdaus, Y.; Le Corre, V. M.; Khan, J. I.; Kan, Z.; Laquai, F.; Beaujuge, P. M.; Anthopoulos, T. D. Key Parameters Requirements for Non-Fullerene-Based Organic Solar Cells with Power Conversion Efficiency> 20%. *Adv. Sci.* **2019**, *6* (9), 1802028.

(7) Li, S.; Li, C.-Z.; Shi, M.; Chen, H. New Phase for Organic Solar Cell Research: Emergence of Y-Series Electron Acceptors and Their Perspectives. *ACS Energy Lett.* **2020**, *5* (5), 1554−1567.

(8) Duan, C.; Zhong, C.; Huang, F.; Cao, Y. Interface Engineering for High Performance Bulk-Heterojunction Polymeric Solar Cells. In *Organic Solar Cells: Materials and Device Physics*; Choy, W. C. H., Ed.; Springer: London, 2013; pp 43−79.

(9) Small, C. E.; Chen, S.; Subbiah, J.; Amb, C. M.; Tsang, S.-W.; Lai, T.-H.; Reynolds, J. R.; So, F. High-efficiency inverted dithienogermole−thienopyrrolodione-based polymer solar cells. *Nat. Photonics* **2012**, *6* (2), 115−120.

(10) Huang, F.; Wu, H. B.; Wang, D.; Yang, W.; Cao, Y. Novel electroluminescent conjugated polyelectrolytes based on polyfluorene. *Chem. Mater.* **2004**, *16* (4), 708−716.

(11) Zhang, Z. G.; Qi, B. Y.; Jin, Z. W.; Chi, D.; Qi, Z.; Li, Y. F.; Wang, J. Z. Perylene diimides: a thickness-insensitive cathode interlayer for high performance polymer solar cells. *Energy Environ. Sci.* **2014**, *7* (6), 1966−1973.

(12) Tan, W. Y.; Wang, R.; Li, M.; Liu, G.; Chen, P.; Li, X. C.; Lu, S. M.; Zhu, H. L.; Peng, Q. M.; Zhu, X. H.; Chen, W.; Choy, W. C. H.; Li, F.; Peng, J. B.; Cao, Y. Lending Triarylphosphine Oxide to Phenanthroline: a Facile Approach to High-Performance Organic Small-Molecule Cathode Interfacial Material for Organic Photovoltaics utilizing Air-Stable Cathodes. *Adv. Funct. Mater.* **2014**, *24* (41), 6540−6547.

(13) Seitkhan, A.; Neophytou, M.; Kirkus, M.; Abou-Hamad, E.; Hedhili, M. N.; Yengel, E.; Firdaus, Y.; Faber, H.; Lin, Y.; Tsetseris, L.; et al. Use of the Phen-NaDPO: Sn (SCN) 2 Blend as Electron Transport Layer Results to Consistent Efficiency Improvements in Organic and Hybrid Perovskite Solar Cells. *Adv. Funct. Mater.* **2019**, *29* (49), 1905810.

(14) Zeng, M.; Wang, X.; Ma, R.; Zhu, W.; Li, Y.; Chen, Z.; Zhou, J.; Li, W.; Liu, T.; He, Z.; Yan, H.; Huang, F.; Cao, Y. Dopamine Semiquinone Radical Doped PEDOT:PSS: Enhanced Conductivity, Work Function and Performance in Organic Solar Cells. *Adv. Energy Mater.* **2020**, *10*, 2000743.

(15) Zheng, Z.; Hu, Q.; Zhang, S.; Zhang, D.; Wang, J.; Xie, S.; Wang, R.; Qin, Y.; Li, W.; Hong, L.; Liang, N.; Liu, F.; Zhang, Y.; Wei, Z.; Tang, Z.; Russell, T. P.; Hou, J.; Zhou, H. A Highly Efficient Non-Fullerene Organic Solar Cell with a Fill Factor over 0.80 Enabled by a Fine-Tuned Hole-Transporting Layer. *Adv. Mater.* **2018**, *30* (34), 1801801.

(16) Tan, J. K.; Png, R. Q.; Zhao, C.; Ho, P. K. H. Ohmic transition at contacts key to maximizing fill factor and performance of organic solar cells. *Nat. Commun.* **2018**, *9* (1), 3269.

(17) Li, G.; Shrotriya, V.; Huang, J. S.; Yao, Y.; Moriarty, T.; Emery, K.; Yang, Y. High-efficiency solution processable polymer photovoltaic cells by self-organization of polymer blends. *Nat. Mater.* **2005**, *4* (11), 864−868.

(18) Wijeyasinghe, N.; Regoutz, A.; Eisner, F.; Du, T.; Tsetseris, L.; Lin, Y.-H.; Faber, H.; Pattanasattayavong, P.; Li, J.; Yan, F.; McLachlan, M. A.; Payne, D. J.; Heeney, M.; Anthopoulos, T. D. Copper(I) Thiocyanate (CuSCN) Hole-Transport Layers Processed from Aqueous Precursor Solutions and Their Application in Thin-Film Transistors and Highly Efficient Organic and Organometal Halide Perovskite Solar Cells. *Adv. Funct. Mater.* **2017**, *27* (35), 1701818.

(19) de Jong, M. P.; van Ijzendoorn, L. J.; de Voigt, M. J. A. Stability of the interface between indium-tin-oxide and poly(3,4-ethylenedioxythiophene)/poly(styrenesulfonate) in polymer light-emitting diodes. *Appl. Phys. Lett.* **2000**, *77* (14), 2255−2257.

(20) Al-Ashouri, A.; Magomedov, A.; Ross, M.; Jost, M.; Talaikis, M.; Chistiakova, G.; Bertram, T.; Marquez, J. A.; Kohnen, E.; Kasparavicius, E.; Levcenco, S.; Gil-Escrig, L.; Hages, C. J.; Schlatmann, R.; Rech, B.; Malinauskas, T.; Unold, T.; Kaufmann, C. A.; Korte, L.; Niaura, G.; Getautis, V.; Albrecht, S. Conformal monolayer contacts with lossless interfaces for perovskite single junction and monolithic tandem solar cells. *Energy Environ. Sci.* **2019**, *12* (11), 3356−3369.

(21) Zhou, Z. M.; Pang, S. P. Highly efficient inverted hole-transport-layer-free perovskite solar cells. *J. Mater. Chem. A* **2020**, *8* (2), 503−512.

(22) Yip, H. L.; Jen, A. K. Y. Recent advances in solution-processed interfacial materials for efficient and stable polymer solar cells. *Energy Environ. Sci.* **2012**, *5* (3), 5994−6011.

(23) Monson, T. C.; Lloyd, M. T.; Olson, D. C.; Lee, Y. J.; Hsu, J. W. P. Photocurrent Enhancement in Polythiophene- and Alkanethiol-Modified ZnO Solar Cells. *Adv. Mater.* **2008**, *20* (24), 4755−4759.

(24) Zhang, S. H.; Zhan, L. L.; Li, S. X.; Li, C. Z.; Chen, H. Z. Enhanced performance of inverted non-fullerene organic solar cells through modifying zinc oxide surface with self-assembled monolayers. *Org. Electron.* **2018**, *63*, 143−148.

(25) Kim, J. S.; Park, J. H.; Lee, J. H.; Jo, J.; Kim, D. Y.; Cho, K. Control of the electrode work function and active layer morphology via surface modification of indium tin oxide for high efficiency organic photovoltaics. *Appl. Phys. Lett.* **2007**, *91* (11), 112111.

(26) Das, S.; Joslin, J.; Alford, T. L. Self-assembled monolayer modified ITO in P3HT:PC61BM organic solar cells with improved efficiency. *Sol. Energy Mater. Sol. Cells* **2014**, *124*, 98−102.

(27) Li, A. Y.; Nie, R. M.; Deng, X. Y.; Wei, H. X.; Zheng, S. Z.; Li, Y. Q.; Tang, J. X.; Wong, K. Y. Highly efficient inverted organic solar cells using amino acid modified indium tin oxide as cathode. *Appl. Phys. Lett.* **2014**, *104* (12), 123303.

(28) Hains, A. W.; Liu, J.; Martinson, A. B. F.; Irwin, M. D.; Marks, T. J. Anode Interfacial Tuning via Electron-Blocking/Hole-Transport Layers and Indium Tin Oxide Surface Treatment in Bulk-

https://dx.doi.org/10.1021/acsenergylett.0c01421
ACS Energy Lett. 2020, 5, 2935−2944

Heterojunction Organic Photovoltaic Cells. *Adv. Funct. Mater.* **2010**, *20* (4), 595−606.
(29) Xu, X.; Xiao, J.; Zhang, G.; Wei, L.; Jiao, X.; Yip, H.-L.; Cao, Y. Interface-enhanced organic solar cells with extrapolated T80 lifetimes of over 20 years. *Sci. Bull.* **2020**, *65* (3), 208−216.
(30) Yip, H. L.; Hau, S. K.; Baek, N. S.; Jen, A. K. Y. Self-assembled monolayer modified ZnO/metal bilayer cathodes for polymer/fullerene bulk-heterojunction solar cells. *Appl. Phys. Lett.* **2008**, *92* (19), 193313.
(31) Yip, H. L.; Hau, S. K.; Baek, N. S.; Ma, H.; Jen, A. K. Y. Polymer solar cells that use self-assembled-monolayer-modified ZnO/Metals as cathodes. *Adv. Mater.* **2008**, *20* (12), 2376.
(32) Wong, W. W. H.; Rudd, S.; Ostrikov, K.; Ramiasa-MacGregor, M.; Subbiah, J.; Vasilev, K. Plasma deposition of organic polymer films for solar cell applications. *Org. Electron.* **2016**, *32*, 78−82.
(33) Stubhan, T.; Salinas, M.; Ebel, A.; Krebs, F. C.; Hirsch, A.; Halik, M.; Brabec, C. J. Increasing the Fill Factor of Inverted P3HT:PCBM Solar Cells Through Surface Modification of Al-Doped ZnO via Phosphonic Acid-Anchored C60 SAMs. *Adv. Energy Mater.* **2012**, *2* (5), 532−535.
(34) Pujari, S. P.; Scheres, L.; Marcelis, A. T.; Zuilhof, H. Covalent surface modification of oxide surfaces. *Angew. Chem., Int. Ed.* **2014**, *53* (25), 6322−56.
(35) Hotchkiss, P. J.; Jones, S. C.; Paniagua, S. A.; Sharma, A.; Kippelen, B.; Armstrong, N. R.; Marder, S. R. The modification of indium tin oxide with phosphonic acids: mechanism of binding, tuning of surface properties, and potential for use in organic electronic applications. *Acc. Chem. Res.* **2012**, *45* (3), 337−46.
(36) Chastain, J. *Handbook of X-ray photoelectron spectroscopy*; Perkin-Elmer Corporation, 1992; Vol. *40*, p 221.
(37) Beamson, G. High resolution XPS of organic polymers. *Scienta ESCA 300 Database*, 1992.
(38) Wagstaffe, M.; Thomas, A. G.; Jackman, M. J.; Torres-Molina, M.; Syres, K. L.; Handrup, K. An experimental investigation of the adsorption of a phosphonic acid on the anatase TiO2 (101) surface. *J. Phys. Chem. C* **2016**, *120* (3), 1693−1700.
(39) Davies, P. R.; Newton, N. G. The chemisorption of organophosphorus compounds at an Al (1 1 1) surface. *Appl. Surf. Sci.* **2001**, *181* (3−4), 296−306.
(40) Kang, M.-S.; Ma, H.; Yip, H.-L.; Jen, A. K. Y. Direct surface functionalization of indium tin oxide via electrochemically induced assembly. *J. Mater. Chem.* **2007**, *17* (33), 3489−3492.
(41) Paniagua, S. A.; Li, E.; Marder, S. R. Adsorption studies of a phosphonic acid on ITO: film coverage, purity, and induced electronic structure changes. *Phys. Chem. Chem. Phys.* **2014**, *16* (7), 2874−2881.
(42) Paniagua, S. A.; Hotchkiss, P. J.; Jones, S. C.; Marder, S. R.; Mudalige, A.; Marrikar, F. S.; Pemberton, J. E.; Armstrong, N. R. Phosphonic acid modification of indium- tin oxide electrodes: combined XPS/UPS/contact angle studies. *J. Phys. Chem. C* **2008**, *112* (21), 7809−7817.
(43) Seah, M. Simple universal curve for the energy-dependent electron attenuation length for all materials. *Surf. Interface Anal.* **2012**, *44* (10), 1353−1359.
(44) Hotchkiss, P. J.; Li, H.; Paramonov, P. B.; Paniagua, S. A.; Jones, S. C.; Armstrong, N. R.; Bredas, J. L.; Marder, S. R. Modification of the Surface Properties of Indium Tin Oxide with Benzylphosphonic Acids: A Joint Experimental and Theoretical Study. *Adv. Mater.* **2009**, *21* (44), 4496.
(45) Owens, D. K.; Wendt, R. C. Estimation of the surface free energy of polymers. *J. Appl. Polym. Sci.* **1969**, *13* (8), 1741−1747.
(46) Jiang, K.; Wei, Q. Y.; Lai, J. Y. L.; Peng, Z. X.; Kim, H.; Yuan, J.; Ye, L.; Ade, H.; Zou, Y. P.; Yan, H. Alkyl Chain Tuning of Small Molecule Acceptors for Efficient Organic Solar Cells. *Joule* **2019**, *3* (12), 3020−3033.
(47) Pettersson, L. A. A.; Roman, L. S.; Inganas, O. Modeling photocurrent action spectra of photovoltaic devices based on organic thin films. *J. Appl. Phys.* **1999**, *86* (1), 487−496.
(48) Kyaw, A. K.; Wang, D. H.; Gupta, V.; Leong, W. L.; Ke, L.; Bazan, G. C.; Heeger, A. J. Intensity dependence of current-voltage characteristics and recombination in high-efficiency solution-processed small-molecule solar cells. *ACS Nano* **2013**, *7* (5), 4569−77.
(49) Firdaus, Y.; Maffei, L. P.; Cruciani, F.; Muller, M. A.; Liu, S. J.; Lopatin, S.; Wehbe, N.; Ndjawa, G. O. N.; Amassian, A.; Laquai, F.; Beaujuge, P. M. Polymer Main-Chain Substitution Effects on the Efficiency of Nonfullerene BHJ Solar Cells. *Adv. Energy Mater.* **2017**, *7* (21), 1700834.
(50) Shuttle, C. G.; O'Regan, B.; Ballantyne, A. M.; Nelson, J.; Bradley, D. D. C.; Durrant, J. R. Bimolecular recombination losses in polythiophene: Fullerene solar cells. *Phys. Rev. B: Condens. Matter Mater. Phys.* **2008**, *78* (11), 113201.
(51) Yao, E. P.; Chen, C. C.; Gao, J.; Liu, Y. S.; Chen, Q.; Cai, M.; Hsu, W. C.; Hong, Z. R.; Li, G.; Yang, Y. The study of solvent additive effects in efficient polymer photovoltaics via impedance spectroscopy. *Sol. Energy Mater. Sol. Cells* **2014**, *130*, 20−26.
(52) Braun, S.; Salaneck, W. R.; Fahlman, M. Energy-Level Alignment at Organic/Metal and Organic/Organic Interfaces. *Adv. Mater.* **2009**, *21* (14−15), 1450−1472.
(53) Yao, E.-P.; Chen, C.-C.; Gao, J.; Liu, Y.; Chen, Q.; Cai, M.; Hsu, W.-C.; Hong, Z.; Li, G.; Yang, Y. The study of solvent additive effects in efficient polymer photovoltaics via impedance spectroscopy. *Sol. Energy Mater. Sol. Cells* **2014**, *130*, 20−26.
(54) Park, S.; Ahn, H.; Kim, J.-y.; Park, J. B.; Kim, J.; Im, S. H.; Son, H. J. High-Performance and Stable Nonfullerene Acceptor-Based Organic Solar Cells for Indoor to Outdoor Light. *ACS Energy Lett.* **2020**, *5* (1), 170−179.
(55) Zhao, Q. Q.; Xiao, Z.; Qu, J. F.; Liu, L. Z.; Richter, H.; Chen, W.; Han, L.; Wang, M. J.; Zheng, J. M.; Xie, Z. Q.; Ding, L. M.; He, F. Elevated Stability and Efficiency of Solar Cells via Ordered Alloy Co-Acceptors. *Acs Energy Lett.* **2019**, *4* (5), 1106−1114.
(56) McNeill, C. R.; Hwang, I.; Greenham, N. C. Photocurrent transients in all-polymer solar cells: Trapping and detrapping effects. *J. Appl. Phys.* **2009**, *106* (2), 024507.
(57) Xiao, J. Y.; Ren, M. R.; Zhang, G. C.; Wang, J. B.; Zhang, D. L.; Liu, L. L.; Li, N.; Brabec, C. J.; Yip, H. L.; Cao, Y. An Operando Study on the Photostability of Nonfullerene Organic Solar Cells. *Solar Rrl* **2019**, *3* (7), 1900077.
(58) Tremolet de Villers, B. J.; MacKenzie, R. C.; Jasieniak, J. J.; Treat, N. D.; Chabinyc, M. L. Linking Vertical Bulk-Heterojunction Composition and Transient Photocurrent Dynamics in Organic Solar Cells with Solution-Processed MoOx Contact Layers. *Adv. Energy Mater.* **2014**, *4* (5), 1301290.
(59) Clarke, T. M.; Lungenschmied, C.; Peet, J.; Drolet, N.; Mozer, A. J. A Comparison of Five Experimental Techniques to Measure Charge Carrier Lifetime in Polymer/Fullerene Solar Cells. *Adv. Energy Mater.* **2015**, *5* (4), 1401345.

https://dx.doi.org/10.1021/acsenergylett.0c01421
ACS Energy Lett. 2020, 5, 2935−2944